

Envelope frequency response function calculation of uncertain structures

D. Moens*, D. Vandepitte

Department of Mechanical Engineering, division PMA, K.U.Leuven, Belgium

e-mail : david.moens@mech.kuleuven.ac.be

Abstract

Requirements for the dynamic properties of a mechanical structure are commonly expressed in terms of eigenfrequencies. Therefore, during the design phase of a mechanical structure much attention is paid to natural frequencies and mode shapes. However, these modal properties tend to vary strongly if small variations are applied on the design model. Therefore, the presence of open design decisions or other uncertain parameters complicates strongly a meaningful dynamic design validation in an early design stage. A fuzzy finite element method for the eigenvalue analysis has been developed to cope with this problem. This method results in fuzzily defined modal properties indicating the degree of uncertainty on the eigenfrequencies and eigenmodes resulting from the uncertain model. However, rather than eigenfrequencies, the specification of responses at frequencies that are critical in the operating conditions of the structure would be a more realistic concept for dynamic design requirements. In order to facilitate the use of such design requirements, a tool is needed to analyze the influence of design decisions on responses at these specific frequencies. Therefore a method for the calculation of fuzzy frequency response functions of uncertain structures is presented. The procedure calculates guaranteed bounds on the envelope on the response function starting from interval bounded uncertainties on the input model. It necessitates the calculation of guaranteed boundaries on the contribution of each individual mode to the total frequency response function.

1. Introduction

During the design optimisation and validation phase, a sound knowledge of the expected dynamic properties and their dependency on design decisions is primordial. Restricting the evaluation to one deterministic analysis in most cases will not be sufficient. In general, when uncertainties exist on the definition of a model (which is nearly always the case) the calculation of the exact probabilistic description on the result of dynamical analyses is only possible through probabilistic methods. However, not every uncertainty in an early design stage can be formulated in a probabilistic manner. Therefore, the probabilistic result may be incorrect and lead to false conclusions as indicated in [1]. The recently introduced fuzzy finite element (FFE) method [2] addresses this problem since it is capable of handling linguistic and therefore more realistic uncertainty descriptions.

The main idea of FFE is to incorporate the fuzzy model parameters in the classic deterministic analysis procedure. Starting from the fuzzy input parameters,

fuzzy system matrices are assembled applying basic operations on the fuzzy model properties. The further analysis is based on the fuzzy system matrices. Historically, a number of concepts has been introduced to perform calculations on fuzzy variables. The most widely known concept consists of a sequence of max-min operations on a numerical representation of the membership functions of the fuzzy parameters. Since the size of the representation of the fuzzy result grows exponentially with every operation, this concept is rarely applied in large numerical computations. The α -sublevel technique is a valuable alternative. It subdivides the membership range into a number of α -levels. The intersection with the membership function at each level results in an interval. At each α -sublevel, an interval analysis is performed, resulting in a new interval at the corresponding α -level. The intervals at all α -sublevels compose the resulting membership function. Figure 1 illustrates this procedure. The main problem now is how to calculate the result of a function of interval defined variables. Basically, this is a bounded optimisation problem. Any kind of optimisation procedure is applicable. However, with growing complexity of the goal function,

*Research Assistant of the Fund for Scientific Research - Flanders (Belgium)(F.W.O)

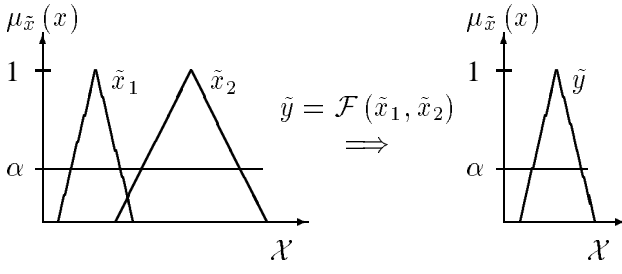


Figure 1: Calculation of the result of the function \mathcal{F} using the α -sublevel technique

the occurrence of local optima complicates the exact solution of the optimisation. The vertex method approximates the resulting interval observing the possible results of the goal function for all combinations of boundary values on the input intervals. This method is not capable of finding local optima since it is based on a number of samples rather than an optimisation procedure. Therefore, it is not safe to apply this procedure from design validation point of view. This paper proposes a method for the calculation of the envelope FRF resulting from an interval defined model. It does not calculate the exact envelope, but ensures guaranteed bounds on the envelope, and therefore is safely applicable for design validation purposes.

2. Envelope FRF approximation

2.1 Problem definition

Considering the first n modes, the amplitude of the frequency response function between node j and k equals

$$\|FRF_{jk}\| = \left| \frac{X_j}{F_k} \right| \quad (1)$$

$$= \left| \sum_{i=1}^n \frac{\phi_{ik} \phi_{ij}}{\phi_i^T K \phi_i - \omega^2 \phi_i^T M \phi_i} \right| \quad (2)$$

with K and M the stiffness and damping matrix and $\phi_i = [\phi_{i1}, \dots, \phi_{in}]^T$ the i -th eigenvector. Simplification of (2) yields

$$\|FRF_{jk}\| = \left| \sum_{i=1}^n \frac{1}{\hat{k}_i - \omega^2 \hat{m}_i} \right| \quad (3)$$

with \hat{k}_i and \hat{m}_i the normalised modal parameters

$$\hat{k}_i = \frac{\phi_i^T K \phi_i}{\phi_{ij} \phi_{ik}} \quad (4)$$

$$\hat{m}_i = \frac{\phi_i^T M \phi_i}{\phi_{ij} \phi_{ik}} \quad (5)$$

The model contains m uncertain parameters β_i , each bounded to an interval B_i , expressed as $\beta \in B$ with $\beta = [\beta_1, \dots, \beta_m]^T$ and $B = [B_1, \dots, B_m]^T$.

The bounds on the amplitude of the total FRF are

$$\overline{\|FRF_{jk}\|} = \max_{\beta \in B} \left| \sum_{i=1}^n \frac{1}{\hat{k}_i - \omega^2 \hat{m}_i} \right| \quad (6)$$

$$\underline{\|FRF_{jk}\|} = \min_{\beta \in B} \left| \sum_{i=1}^n \frac{1}{\hat{k}_i - \omega^2 \hat{m}_i} \right| \quad (7)$$

The dependency of the total FRF to the uncertain parameters β is implicit through the normalised modal parameters, which depend on the uncertain parameters through the model properties incorporated in K and M and their corresponding eigenvectors as expressed in (4) and (5). Therefore, the solution of the optimisation stated in (6) and (7) through classic iterative procedures is computationally intensive and time-consuming. It cannot be efficiently solved using classic optimisation strategies. It has been shown in [3] that an approximative optimisation procedure results in safe boundaries on the total FRF envelope expressed as

$$\overline{\overline{FRF_{jk}}} = \sum_{i=1}^n \overline{\overline{FRF_{jk_i}}} \quad (8)$$

$$\underline{\underline{FRF_{jk}}} = \sum_{i=1}^n \underline{\underline{FRF_{jk_i}}} \quad (9)$$

with $\overline{\overline{FRF_{jk_i}}}$ and $\underline{\underline{FRF_{jk_i}}}$ describing guaranteed upper respectively lower bounds on the envelope of the i -th mode FRF. The calculation of these guaranteed bounds on the single mode envelope FRF is based on the exact single mode envelope FRF description

$$\overline{\overline{FRF_{jk_i}}} = \frac{1}{\min_{\beta \in B} (\hat{k}_i - \omega^2 \hat{m}_i)} \quad (10)$$

$$\underline{\underline{FRF_{jk_i}}} = \frac{1}{\max_{\beta \in B} (\hat{k}_i - \omega^2 \hat{m}_i)} \quad (11)$$

Introducing the goal function $\mathcal{F}(\omega) = (\hat{k}_i(\beta) - \omega^2 \hat{m}_i(\beta))$, the optimisation mathematically expressed as

$$\overline{\mathcal{F}}(\omega) = \max_{\beta \in B} (\hat{k}_i(\beta) - \omega^2 \hat{m}_i(\beta)) \quad (12)$$

$$\underline{\mathcal{F}}(\omega) = \min_{\beta \in B} (\hat{k}_i(\beta) - \omega^2 \hat{m}_i(\beta)) \quad (13)$$

is the core of the single mode envelope FRF calculation. Since (8) and (9) use guaranteed bounds on the

envelope, guaranteed bounds $\overline{\overline{\mathcal{F}(\omega)}}$ and $\underline{\underline{\mathcal{F}(\omega)}}$ on the optimised goal function $\mathcal{F}(\omega)$ obeying

$$\overline{\overline{\mathcal{F}(\omega)}} \geq \overline{\mathcal{F}(\omega)} \quad (14)$$

$$\underline{\underline{\mathcal{F}(\omega)}} \leq \underline{\mathcal{F}(\omega)}. \quad (15)$$

are calculated. Inverting these guaranteed bounds on the goal function $\mathcal{F}(\omega)$ results in guaranteed bounds on the single mode envelope FRF. The next part of this paper describes how to calculate $\overline{\overline{\mathcal{F}(\omega)}}$ and $\underline{\underline{\mathcal{F}(\omega)}}$.

2.2 Solution procedures

Equations (12) and (13) indicate that the global optimisation problem of (6) and (7) is decomposed into $2n$ independent optimisation problems (2 for each mode). For the sake of clarity, this part of the paper omits the index i , assuming that everything accounts for each individual mode.

It is impossible to perform the optimisation stated in (12) and (13) for all frequencies within the analysed frequency band. The most straightforward solution strategy is to perform the optimisation for a limited number of discrete frequencies, and construct an approximation for $\overline{\mathcal{F}(\omega)}$ and $\underline{\mathcal{F}(\omega)}$ interpolating through the results of these discrete optimisations. In order to ensure that this interpolation results in a safe approximation for all intermediate frequencies, a quadratic interpolation scheme is applied:

1. Define a grid in the frequency domain consisting of ν frequencies: $[\omega_1, \dots, \omega_\nu]$.
2. Perform the optimisation of the goal function \mathcal{F} for these frequencies:

$$\max_{\beta \in B} \mathcal{F}(\omega_i) = \overline{\mathcal{F}}_i$$

$$\min_{\beta \in B} \mathcal{F}(\omega_i) = \underline{\mathcal{F}}_i$$

3. Compose an approximation for the optimised goal function for all intermediate frequencies using

$$\overline{\overline{\mathcal{F}(\omega)}} = \frac{(\omega_{i+1}^2 - \omega^2) \overline{\mathcal{F}}_i + (\omega^2 - \omega_i^2) \overline{\mathcal{F}}_{i+1}}{\omega_{i+1}^2 - \omega_i^2}$$

$$\underline{\underline{\mathcal{F}(\omega)}} = \frac{(\omega_{i+1}^2 - \omega^2) \underline{\mathcal{F}}_i + (\omega^2 - \omega_i^2) \underline{\mathcal{F}}_{i+1}}{\omega_{i+1}^2 - \omega_i^2}$$

for all $\omega \in [\omega_i, \omega_{i+1}]$

A graphical representation of the single mode goal function clarifies why the quadratic interpolation procedure ensures guaranteed upper and lower bounds on the exact interval. Consider a 2 dimensional workspace in \hat{k} and \hat{m} . In this workspace, for one given value of ω , the goal function is represented by a straight line, expressed as

$$\hat{k} - \omega^2 \hat{m} = \mathcal{F}^*. \quad (16)$$

All \hat{k}, \hat{m} -pairs on this line represent structures with equal values \mathcal{F}^* for the goal function. The goal function can be graphically interpreted as the intersection point of the line represented by (16) and the \hat{k} -axis, as indicated in Figure 2.

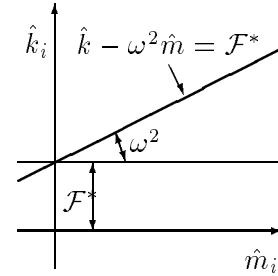


Figure 2: Graphical interpretation of the goal function

The \hat{k}, \hat{m} -combinations resulting from all possible combinations of input uncertainties β belong to a restricted domain in the \hat{k}, \hat{m} -workspace:

$$\langle \hat{k}, \hat{m} \rangle_\beta = \left\{ \left(\hat{k}(\beta), \hat{m}(\beta) \right), \beta \in B \right\}. \quad (17)$$

Optimising the goal function for one specific value of ω is graphically equivalent to constructing both lines with a slope ω^2 tangent to $\langle \hat{k}, \hat{m} \rangle_\beta$ (one for the maximisation, one for the minimisation). The optimisation for $\omega = 0 \rightarrow \infty$ is equivalent to circumscribing $\langle \hat{k}, \hat{m} \rangle_\beta$ by straight lines tangent to this domain with slopes ranging from 0 to 90°. Using this concept, the optimisation is straightforward if an exact analytical description of the border of $\langle \hat{k}, \hat{m} \rangle_\beta$ is available. Since this is generally not the case, an approximate procedure based on a polygonal circumscription of $\langle \hat{k}, \hat{m} \rangle_\beta$ is introduced. The polygon consists of a limited number 2ν of lines tangent to $\langle \hat{k}, \hat{m} \rangle_\beta$. Since each borderline of the polygon is tangent to $\langle \hat{k}, \hat{m} \rangle_\beta$, the goal functions represented by these lines are optimal at their according frequencies $\omega_i, i = 1 \dots \nu$. Therefore, the borderlines are expressed as

$$\hat{k} - \omega_i^2 \hat{m} = \overline{\mathcal{F}}_i, i = 1 \dots \nu \quad (18)$$

$$\hat{k} - \omega_i^2 \hat{m} = \underline{\mathcal{F}}_i, i = 1 \dots \nu. \quad (19)$$

These lines represent the result of steps 1 and 2 in the interpolation procedure. Now consider a frequency $\omega^* \in [\omega_i, \omega_{i+1}]$. The results of the exact optimisation would be represented by lines with gradient ω^{*2} tangent to $\langle \hat{k}, \hat{m} \rangle_\beta$. An approximation of the optimal goal function is calculated constructing lines with this gradient through the intersection point of the graphical representation of the optimised goal functions $\mathcal{F}(\omega_i)$ and $\mathcal{F}(\omega_{i+1})$. Since $\langle \hat{k}, \hat{m} \rangle_\beta$ is completely contained within the polygonal circumscription, this approximation is on the safe side of the exact (unknown) optimised goal function. This is illustrated in figure 3. Note that in this figure $\overline{\mathcal{F}}(\omega^*)$ is unknown but safely overestimated by $\overline{\overline{\mathcal{F}}}(\omega^*)$.

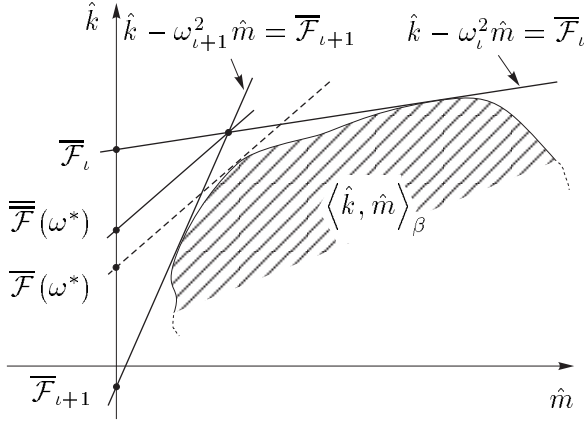


Figure 3: Safe approximations using the circumscribing polygon

Repeating this procedure for all intermediate frequencies results in an approximation of the optimised goal function using the cornerpoints of the circumscribing polygon. This is mathematically equivalent to the quadratic interpolation in step 3 of the interpolation procedure. Figure 4 clarifies the graphical interpretation of the interpolation procedure for $\nu = 4, \omega_1 = 0$ and $\omega_\nu = \infty$.

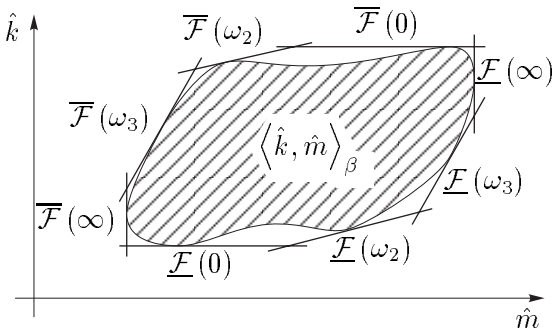


Figure 4: Approximate circumscribing polygon

This paper describes three approximated optimisation strategies. Each of these strategies constructs a polygon in the \hat{k}, \hat{m} -space which approximates the exact domain by a limited number of straight lines tangent to $\langle \hat{k}, \hat{m} \rangle_\beta$.

2.2.1 Corner method

The corner method creates a rectangular circumscription of $\langle \hat{k}, \hat{m} \rangle_\beta$ using the optimisation of $\mathcal{F}(0)$ and $\mathcal{F}(\infty)$. From the definition of $\mathcal{F}(\omega)$ it is clear that this is the independent optimisation of the normalised modal parameters:

$$\underline{\mathcal{F}}(0) = \min_{\beta \in B} \hat{k} \quad (20)$$

$$\overline{\mathcal{F}}(0) = \max_{\beta \in B} \hat{k} \quad (21)$$

$$\underline{\mathcal{F}}(\infty) \leftrightarrow \max_{\beta \in B} \hat{m} \quad (22)$$

$$\overline{\mathcal{F}}(\infty) \leftrightarrow \min_{\beta \in B} \hat{m}. \quad (23)$$

Figure 5 displays the resulting rectangular region.

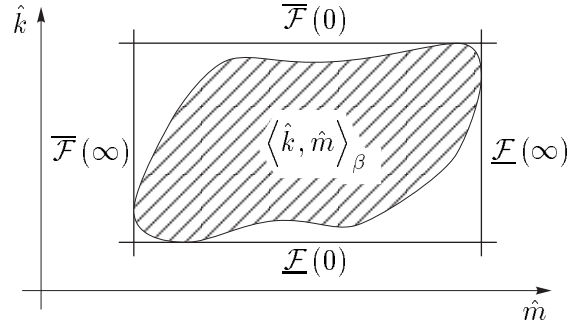


Figure 5: Graphical interpretation of the corner method

2.2.2 Corner-Eigenvalue method

The corner eigenvalue method adds the results of the eigenvalue optimisation to the rectangular area of the corner method:

$$\bar{\lambda} = \max_{\beta \in B} \left(\frac{\hat{k}}{\hat{m}} \right) \quad (24)$$

$$\underline{\lambda} = \min_{\beta \in B} \left(\frac{\hat{k}}{\hat{m}} \right). \quad (25)$$

From (24) and (25) it is clear that the lines expressed as

$$\hat{k} = \bar{\lambda} \hat{m} \quad (26)$$

$$\hat{k} = \underline{\lambda} \hat{m} \quad (27)$$

add new delimiters to the rectangular circumscription of $\langle \hat{k}, \hat{m} \rangle_\beta$. This is indicated in Figure 6.

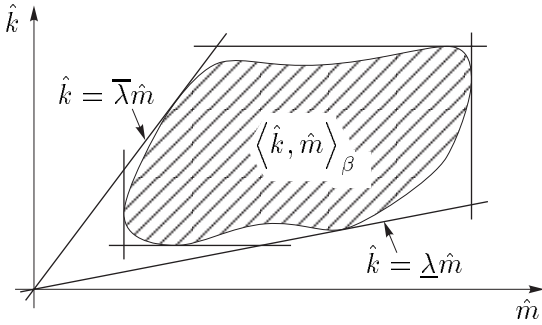


Figure 6: Graphical interpretation of the corner eigenvalue method

2.2.3 Optimised Vertex method

The vertex method applied to the single mode FRF optimisation is basically an approximation of $\langle \hat{k}, \hat{m} \rangle_\beta$ combining the results of all possible combinations of boundary values on the input uncertainties. This method does not ensure a circumscription of $\langle \hat{k}, \hat{m} \rangle_\beta$ since the analysed input boundary combinations do not necessarily include the global extremities of the goal function. Therefore, an extra optimisation step is added. The goal function is optimised using the gradient of each line from the approximative area resulting from the vertex method. This method is safe, but requires an unknown number of optimisations.

3. Numerical Example

The numerical example consists of a series of four masses connected with four springs, as indicated in Figure 7. The structure is undamped. The spring

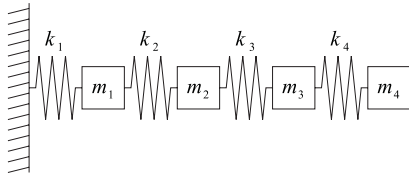


Figure 7: Model for numerical analysis

stiffnesses and masses are uncertain and mutually uncorrelated. Table 1 summarizes the intervals at the analysed α -level.

The polygonal circumscription of $\langle \hat{k}, \hat{m} \rangle_\beta$ is calculated for the FRF between mass 3 and 4. Figure 8

	stiffness (N/m)		mass (kg)		
	lower bound	upper bound		lower bound	upper bound
k_1	1000	1010	m_1	5	6
k_2	1600	1620	m_2	12	14
k_3	3050	3100	m_3	9	10
k_4	2310	2340	m_4	16	18

Table 1: Elemental properties of the reference model

compares this polygon for the three proposed methods for the first mode of this model. They are plotted upon the \hat{k}_1, \hat{m}_1 -pairs resulting from the vertex method. This figure indicates that for this mode, the rectangular area of the corner method is a good approximation of $\langle \hat{k}_1, \hat{m}_1 \rangle_\beta$ since the \hat{k}_1, \hat{m}_1 -pairs resulting from the vertex method describe a quasi rectangular area. Adding the eigenvalue delimiters or applying the optimised vertex method does not substantially decrease the size of the overestimation of $\langle \hat{k}_1, \hat{m}_1 \rangle_\beta$.

Figure 9 compares the circumscribing polygons for the three proposed methods for the fourth mode of this model. They are plotted upon the \hat{k}_4, \hat{m}_4 -pairs resulting from the vertex method. This figure indicates that the $\langle \hat{k}_4, \hat{m}_4 \rangle_\beta$ circumscription of the corner method substantially overestimates the exact domain. Adding the results of the eigenvalue optimisation results in a much closer circumscription. The optimised vertex method results in the closest circumscription.

Figure 10 compares the resulting total FRF's for the three approximate optimisation methods. It is clear that the resulting envelope FRF of the corner method is only useful up to the first eigenfrequency. This is due to the fact that the corner method produced a good approximation of $\langle \hat{k}_1, \hat{m}_1 \rangle_\beta$, but failed to give a close approximation of $\langle \hat{k}, \hat{m} \rangle_\beta$ for the higher modes. The large overestimation for these modes is translated into an envelope FRF ranging from zero to infinity for the main part of the frequency region. Adding the eigenvalue optimisation results makes the resulting envelope FRF much more useful compared to the corner method. The results of the optimised vertex method differ only slightly from those of the corner eigenvalue method.

4. Conclusions

This paper describes a methodology for efficiently calculating guaranteed bounds on an envelope FRF of a fuzzily defined structure. The method is based on a graphical interpretation of the goal function for the single mode envelope FRF calculation. The approximations of the optimisations are safe since the search domain is overestimated. The most straightforward method describes the search domain by a rectangle. The other described methods aim at a decrease of the amount of the overestimation.

The numerical example indicates that the corner eigenvalue method is the most efficient, since it requires a fixed number of six optimisation steps for each mode, while the resulting total envelope FRF does not differ much from the far more intensive optimised vertex method.

References

- [1] I. Elishakoff, D. Duan, *Application of Mathematical Theory of Interval Analysis to Uncertain Vibrations*, Proc. of NOISE-CON 94, Ft. Lauderdale, Florida, pp.519-524 (1994).
- [2] S.S. Rao, J.P. Sawyer, *Fuzzy Finite Element Approach for the Analysis of Imprecisely Defined Systems*, *AIAA Journal*, Vol.33, pp.2364-2370 (1995).
- [3] D. Moens, D. Vandepitte, *A Method for the Calculation of Fuzzy Frequency Response Functions of Uncertain Structures Based on Modal superposition*, Proc. of Euromech 405 Colloquium on Numerical Modeling of Uncertainties, Valenciennes, pp.93-101 (1999).

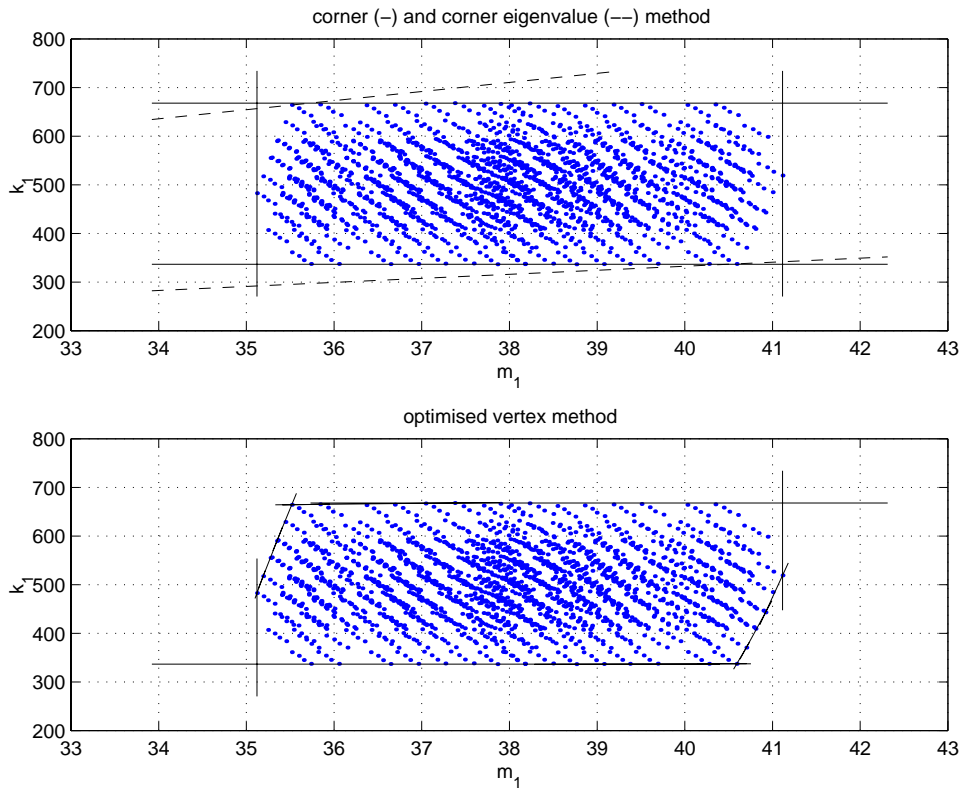


Figure 8: Comparison of $\langle \hat{k}_1, \hat{m}_1 \rangle_\beta$ for the three proposed methods

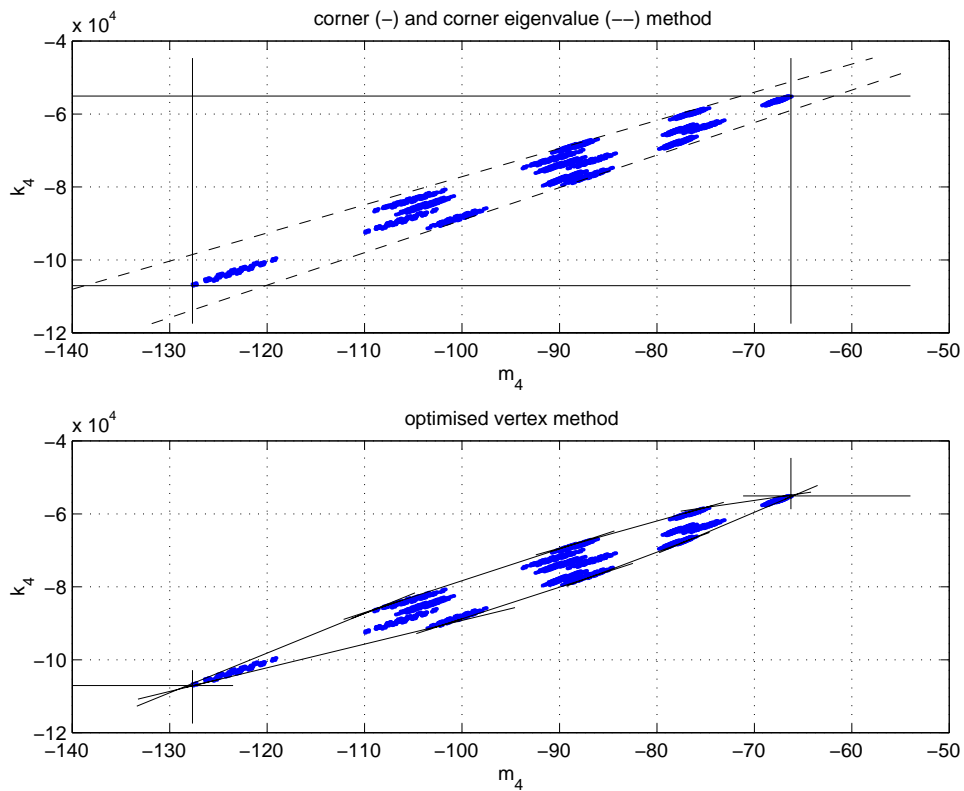


Figure 9: Comparison of $\langle \hat{k}_4, \hat{m}_4 \rangle_\beta$ for the three proposed methods

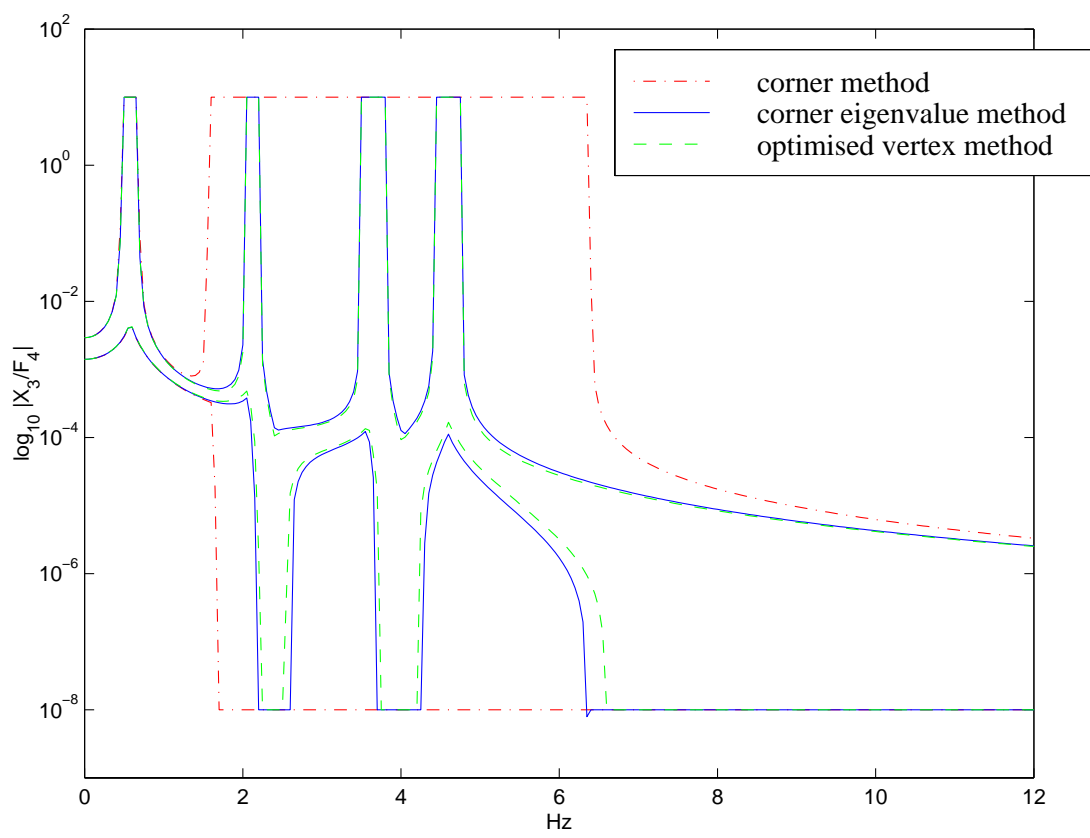


Figure 10: Comparison of the resulting envelope FRF_{34} for the three methods